Proceedings of the ASME 2010 3rd Joint US-European Fluids Engineering Summer Meeting and 8th International Conference on Nanochannels, Microchannels, and Minichannels
FEDSM-ICNMM2010
August 1-5, 2010, Montreal, Canada

FEDSM-ICNMM2010-31166

COMPARISON OF DIFFERENT HEAT EXCHANGER MODELS IN A THERMOACOUSTIC ENGINE SIMULATION

Catherine Weisman*
LIMSI-CNRS and
Université Pierre et Marie Curie
LIMSI-CNRS UPR3251, BP 133
F-91403 Orsay France
Email: catherine.weisman@limsi.fr

Diana Baltean-Carlès
LIMSI-CNRS and
Université Pierre et Marie Curie
LIMSI-CNRS UPR3251, BP 133
F-91403 Orsay France
Email: baltean@limsi.fr

Patrick Le Quéré
LIMSI-CNRS
LIMSI-CNRS UPR3251, BP 133
F-91403 Orsay France
Email: plq@limsi.fr

Luc Bauwens
Mechanical & Manufacturing Engineering
University of Calgary
2500 University Drive NW, Calgary, AB T2N 1N4
Canada
Email: bauwens@ucalgary.ca

ABSTRACT

The role of unavoidable space between heat exchangers and stack inside a thermoacoustic standing wave generator is investigated. A two-dimensional Low Mach number viscous and heat conducting flow model of the active thermoacoustic cell, comprising heater and cooler separated by a stack made of parallel conducting plates, is described. Three different models of heat exchangers are implemented and compared. Ideal heat exchangers consist of a fluid zone with imposed temperature. The other two models are made up of stacks of horizontal plates, either with specified wall temperatures, in one model and with constant prescribed heat fluxes in the other. A multiple scale analysis allows for coupling the active thermoacoustic cell model with the flow inside the resonator, obtained as a solution to a linear acoustic formulation. When a large enough temperature difference is applied between the heat exchangers, initial pressure perturbations grow. Different resonant modes are amplified for different configurations, in the same way as in experimental observations.

INTRODUCTION

A standing wave thermoacoustic engine consists of a long tube with one end closed and equipped with a load such as a piston at the other end, within which a heat exchanger section is placed. The heat exchanger section is made up of a heater and a cooler, separated by a porous medium or a stack, along which surface heat exchange occurs. When a sufficiently large temperature difference is applied between the two heat exchangers, some initial pressure perturbations are amplified by the so-called thermoacoustic instability.

Although in many studies, the complete system is described using one-dimensional models [1–3], a more accurate model of the heat exchanger section requires a multidimensional formulation, because of the strong coupling between the hydrodynamic and temperature fields. Recent studies [4–6] have focused upon heat exchanger design and on thermal edge effects, in particular in the region between the extremities of the stack and the heat exchangers. The present study considers a stack made up of flat horizontal plates of conducting material; it focuses upon the role

*Address all correspondence to this author.

of unavoidable dead space between heat exchangers and stack. The issue is investigated numerically using a two-dimensional Low Mach number viscous and heat conducting flow model of the so-called active thermoacoustic cell, defined as the stack, heater, cooler, and associated dead spaces. Coupling with the flow in the left and right parts of the resonator tubes is dealt with based upon results from a multiple scale analysis. The multiple scale formulation has been described in detail in [7]. In the resonators, the appropriate model consists of an exact linear acoustic solution. Assuming vertical periodicity in the active-cell, i.e. that the flow is identical in different stack or heat exchanger spaces, the simulation domain can be reduced to one slice of the active cell, delimited by two successive stack plates. Three different models of heat exchangers are considered and have been simulated: "ideal" heat exchangers, modeled as a fluid zone within which a constant fluid temperature is prescribed at all times (hot for the heater and cold for the cooler), and two models in which the heat exchangers are made up of stacks of horizontal plates with a prescribed blockage ratio, allowing for porosities that differ between heat exchangers and stack. For the latter geometry, the two models consider respectively fixed, prescribed temperatures in the heat exchangers, and constant prescribed heat fluxes.

The main features of the model, in which an exact analytical solution to the resonator acoustics is coupled to a direct numerical simulation of the viscous and conducting flow in the stack and heat exchangers, are briefly described in the next section. The three models of heat exchangers are also explained in detail. A description of the numerical solution technique follows. Finally, results are presented for a case corresponding to experiments described in the literature [8].

PHYSICAL MODEL

The simulation domain, consisting of one slice of the active cell, delimited by two successive stack half-plates is shown in Fig. 1. In the reference experiment [8] the heat exchangers also consist of stacks of horizontal plates, with different thermophysical properties, different blockage ratio, and different length. The stack and heat exchangers assembly is placed within the resonator, which is closed at one end, while a load is placed at its other end. That device is described by a an initial boundary value problem characterized by conservation of mass, momentum and energy, including viscosity and conduction but no gravity, for a known compressible fluid, over the domain described in Fig. 1, with suitable initial conditions. The appropriate description of the heat exchangers, including thermal boundary conditions, will depend upon the heat exchanger model. This is dealt with in detail below. No-slip boundary conditions are imposed on the heat exchanger and stack walls. In the stack walls, energy is conserved. Temperature and heat flux are continuous along the stack walls. Along the stack plate centerlines, periodic thermal boundary conditions are imposed.

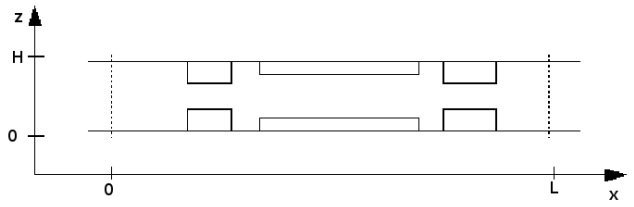

FIGURE 1. Active thermoacoustic cell geometry

Given that the period will be determined by an acoustic resonance, time is scaled by the resonator length L_R divided by the speed of sound at the reference temperature a_{ref}. The length of the heat exchanger section is of the same order as the stack length L_S; it is taken to be much smaller than the length of the resonator. A reference velocity U_{ref} is introduced assuming that the fluid sweeps a length of the order of the length of the heat exchanger section. This results in a reference Mach number $M = U_{ref}/a_{ref} = L_S/L_R$, which is small for short stacks. The Low Mach number model outlined below is explained in detail in [7].

As to initial conditions, given that the focus is currently upon engine start up, in the simulations below, two cases were considered: an initial random noise, or a small amplitude monochromatic acoustic wave.

Multiple Scale Formulation

Scaling length by L_R, time by L_R/a_{ref}, velocity by U_{ref}, the flow in the resonators is found to be governed by usual inviscid, non-conducting, isentropic acoustics. A d'Alembert solution is readily formulated using Riemann variables, $\mathscr{L} = \gamma u - \sqrt{T}p^{(1)}$ and $\mathscr{R} = \gamma u + \sqrt{T}p^{(1)}$ which remain constant on characteristics moving at the speed of sound (the speed of the fluid being negligible in comparison). The temperature T has different values on the two sides of the stack and heat exchangers. u is the velocity, γ is the ratio of specific heats. $p^{(1)}$ is the acoustic pressure, i.e. a perturbation of order M to the mean pressure, which is constant and spatially uniform. $p^{(2)}$ represents the dynamic pressure correction in the heat exchangers, i.e. a perturbation of order M^2 to the mean pressure.

At the closed end $x = x_L$, velocity is zero, $u = 0$, and the outgoing Riemann variable $\mathscr{R}$ is thus determined by a reflection condition: $\mathscr{R}(x_L,t) = -\mathscr{L}(x_L,t)$. At the right end $x = x_R$, the load is described as an impedance f such that $p^{(1)} = fu$, thus yielding a somewhat more complex reflection condition: $\mathscr{L}(x_R,t) = \left(\gamma - f\sqrt{T}\right)/\left(\gamma + f\sqrt{T}\right)\mathscr{R}(x_R,t)$. A closed end ($u = 0$ hence $f \to \infty$) results in $\mathscr{L} = -\mathscr{R}$ (as at the left end) while an open end ($p^{(1)} = 0$ hence $f = 0$) results in $\mathscr{L} = \mathscr{R}$.

Combining the d'Alembert solution with these boundary conditions, the value of one of the Riemann variables at the interface between resonator and heat exchanger can be related to the value of the other one at the same location at an earlier time equal to the current time, minus the round-trip travel time to the respective end.

In the heat exchanger section, the conservation laws are scaled as above except for length which is now scaled by L_S. This produces a viscous, conducting low Mach number model that supports spatially homogeneous pressure fluctuations up to leading order, in which temperatures may vary at leading order and in which dynamically induced pressure gradients only occur at order M^2. In effect, the approximation obtained is the same as in [9–11]. However, given that the acoustic model in the resonator only produces pressure fluctuations at order M, in the current problem, pressure remains constant at leading order. Because the temperatures differ at leading order between the hot and cold heat exchangers, though, leading order temperature and density variations occur. Pressure and densities are related by the ideal gas equation of state in which pressure is taken as its constant leading order value. Thus although this is a low Mach number flow, because leading order density variations occur, energy conservation cannot be decoupled from conservation of mass and momentum. The dimensionless equations become:

$$\frac{\partial \rho}{\partial t} + \nabla.\rho\mathbf{u} = 0 \tag{1}$$

$$\frac{\partial(\rho\mathbf{u})}{\partial t} + \nabla.(\rho\mathbf{u}\otimes\mathbf{u}) = -\nabla p^{(2)} + \frac{1}{Re}\nabla.\tau \tag{2}$$

$$\rho\left[\frac{\partial T}{\partial t} + (\mathbf{u}.\nabla)T\right] = \frac{1}{Pe}\nabla^2 T \tag{3}$$

$$p = 1 = \rho T \tag{4}$$

where $\tau = [\nabla\mathbf{u} + (\nabla\mathbf{u})^t - \frac{2}{3}(\nabla.\mathbf{u})\mathbf{I}]$, the reference Reynolds number is $Re = \rho_{ref}U_{ref}L_S/\mu_{ref}$ and the reference Péclet number is $Pe = \rho_{ref}c_{pref}U_{ref}L_S/k_{ref}$. In the solid stack plates (and if applicable the heat exchanger plates), the dimensionless heat conduction equation is:

$$\frac{\partial T}{\partial t} = \frac{1}{Pe_s}\Delta T, \tag{5}$$

where the solid Péclet number is defined as $Pe_s = Pe\alpha_{ref}/\alpha_s$, α_{ref} and α_s being thermal diffusivities respectively at the reference state in the fluid and in the solid (the value of the solid Péclet number depends on the solid that is considered).

In the outer (acoustic) scaling, the stack and heat exchangers section has a negligible length; in the inner scaling, the resonators have a length that $\to\infty$. Matching the two solutions, first, from the above, the inner section is transparent to acoustic pressure. However, integrating the energy equation over the entire heat exchanger section, of height H, one finds that

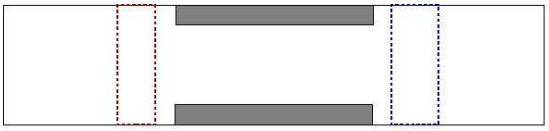

FIGURE 2. Ideal heat exchangers

FIGURE 3. Heat exchangers - constant prescribed heat

$$(u_L - u_R)H + \frac{1}{Pe}\int \nabla T\cdot\mathbf{n}ds = 0 \tag{6}$$

Here, u_L corresponds to a location $x\to-\infty$ in the scaling associated with the heat exchanger section, but to the heat exchanger end of the left side of the resonator. Likewise, u_R corresponds to a location $x\to\infty$ in the scaling associated with the heat exchanger section, but to the heat exchanger end of the right side of the resonator. Thus, while being transparent to acoustic (order M) pressure, the stack and heat exchangers act as a source of velocity in the acoustics, thus coupling the inner and outer problems.

Taking into account that $p^{(1)}$ is spatially uniform in the stack and heat exchangers assembly, Eq. (6), together with the acoustic solution above, provides velocity boundary conditions for $x\to-\infty$ and $x\to+\infty$ in the heat exchanger section, hence allowing for numerical simulation.

Heat Exchanger Models

As already mentioned, three different heat exchanger models were studied.

The first model considers "ideal" heat exchangers. No physical heat exchanger is present; instead, it is assumed that the fluid somehow reaches the specified heat exchanger temperature at all times. In the simulation this is achieved by setting the fluid temperature at a the desired fixed value within a specified "heat exchanger" region, as shown in Fig. 2, instead of solving the energy equation.

In the second model, the heat exchangers are considered to be solid plates maintained at constant temperature (T_{hot} for

the hot heat exchanger, and T_{cold} for the cold heat exchanger). Since the size and number of plates composing the thermoacoustic stack and the heat exchangers can differ, the geometry shown in Fig. 1 includes a different blockage ratio for both sets of stacks. As in the reference experiment [8], the hot and cold heat exchangers have the same blockage ratio. Also, gaps are present on both sides of the stack, between heat exchangers and stack. These gaps are of interest in the current study; they were taken to be equal to the distance between two stack plates.

In the third model, the same geometry is considered, but this time a constant heat flux is imposed along the heat exchanger symmetry plane, as shown in Fig. 3, and conduction within the walls is included in the simulation. The value of the flux for each heat exchanger is calculated so that the total heat flux injected at the corresponding (hot or cold) heat exchanger/fluid interface is the same as in the second model.

In the first model, there are no physical heat exchangers; these are ideal in the sense that the fluid is set to reach exactly the specified "heat exchanger temperatures.". Thus the solution is not constrained by boundary conditions. In the latter two models, the heat exchangers are made up of actual plates. The boundary conditions then provide an accurate description of the actual heat exchange mechanism, and in that sense, they do constrain the problem. These boundary conditions, are, however, representative of the true physics of the heat exchangers. Thus, if in a sense they impose a solution, that solution is representative of real exchangers made up of parallel plates.

In all three models, the heat capacity and thermal conductivity of the wall material are assumed to be independent of temperature.

NUMERICAL SOLUTION

The numerical solution uses a finite volume solver initially developed for direct simulation of non-Boussinesq convection [12]. Treatment of diffusive terms is implicit while convection is explicit. The algorithm is second-order accurate in both space and time. A staggered mesh is used, with velocities defined on cell faces and state variables at cell centers. Continuity is ensured based upon a version of the projection method adapted for variable density, using a fractional step. The Helmholtz equations obtained for temperature and velocity components are solved by either an ADI method or GMRES method (both algorithms are tested). The equation for the dynamic pressure correction is solved using a multigrid method.

The presence of stack and heat exchanger walls is dealt with by introducing a phase variable that differentiates between fluid and solid, and ensures continuity of temperature and of the heat flux vector at the solid/fluid interfaces.

At each time step, resonator acoustics yields, on both sides of the stack and heat exchanger section, a relationship between velocity and acoustic pressure. Equation (6) provides a third relationship, thus yielding the necessary velocity conditions. The three variables (left and right velocity and acoustic pressure at the active cell location) obtained from solving these three equations are also stored for later use in the simulation, providing a discretized version of the analytical solution in the resonators.

In order to provide thermal initial conditions, before starting the simulation proper, a steady state temperature field is determined solving the heat conduction problem assuming that the fluid stays at rest. To that effect, the equations are made dimensionless based on a different reference time scale than that previously defined, corresponding to heat conduction in the gas. Next, that temperature field is used as an initial condition, that may trigger thermoacoustic instability. In the simulation proper, the reference time scale is the acoustic time scale previously defined in the physical model.

RESULTS

The results shown correspond to simulations described in [8]. A device 1 m long with a 3.5 cm stack, filled with helium at given values of mean pressure, that were varied from 0.1 to 0.5 MPa, and 293 K on the cold side was simulated. This corresponds to a dimensionless description in which $L_R = 28.6L_S$, hence a reference Mach number of 0.035. The hot heat exchanger is located at a distance of $0.055L_R$ from the left end. The width of the stack passages is $0.022L_S$ and the plate thickness is $0.008L_S$. The stack is taken to be made of stainless steel, and the heat exchangers are made of nickel. The hot heat exchanger has a length equal to $0.21L_S$, the cold heat exchanger has a length equal to $0.63L_S$, the plates are calculated to be (on average) $0.009L_S$ thick, and the passages $0.021L_S$ wide. The distance between heat exchanger and stack is equal to the stack passage width.

As to resolution, meshes of 512×32, 1024×64 and 512×64 were used. Time steps of about 1/100th of the period were used initially, but as velocities increased, steps smaller by a factor ten were used. These parameters were found to result in adequate convergence.

On a coarse mesh, one simulation, from start up until a periodic regime is observed, takes about 30 hours on a NEC SX8, hence a fairly large computation. An average of 3 or 4 multigrid cycles at every time step are necessary throughout the simulation. For small time steps, the ADI algorithm was found to give identical results to GMRES, and since the exact solution obtained with GMRES required a significantly longer time, the ADI method was used in the simulations shown below. Most simulations shown below took about 20 min CPU time.

Initial Temperature Field

The initial temperature field is the driver of the thermoacoustic instability. The most common initial temperature distribution

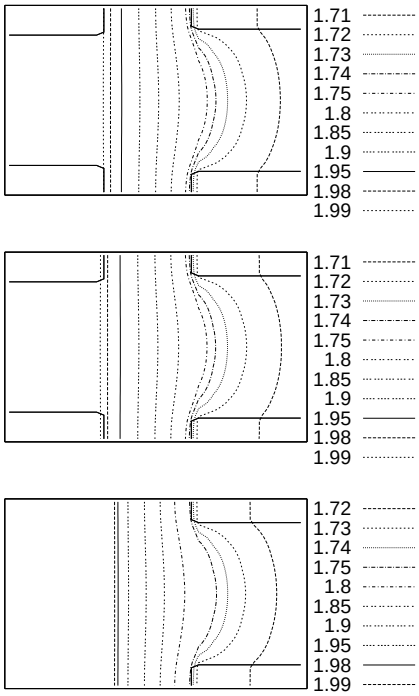

FIGURE 4. Temperature field, Top: model 1, temperature fixed on solid heat exchangers, Middle: model 2, heat flux fixed, Bottom: model 3, ideal heat exchangers

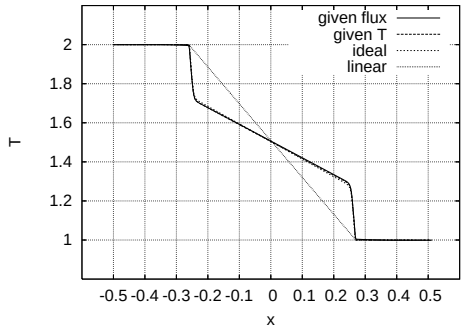

FIGURE 5. Temperature profile along centerline, comparison between heat exchanger models

used for example in 1D studies consists of a homogeneous hot temperature left of the hot heat exchanger, homogeneous cold temperature right of the cold heat exchanger, and linear variation from hot to cold between the two heat exchangers. However, in reality, the temperature field established by pure conduction is not one-dimensional, and these multidimensional effects may play an important role in the instability.

The steady conduction temperature fields obtained for the three models of heat exchangers are shown in Fig. 4, in the

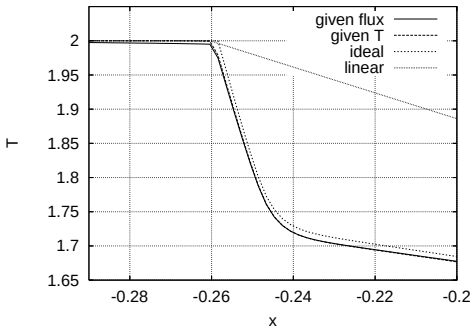

FIGURE 6. Temperature profile along centerline, detail between hot heat exchanger and stack plate, comparison between models

zone between the hot heat exchanger and the stack plate, for $T_{hot} = 2T_{cold}$. Outside the region close to the ends of the stack plates, the steady temperature field is mostly one dimensional. Isothermal lines, shown in Fig. 4, show that the ideal model yields slightly different results than the other two. The temperature profiles obtained from the three models, along a line going through the heat exchanger section that coincides with the stack gap centerline, are shown in Fig. 5 and Fig. 6. The profiles obtained from the latter two models (solid heat exchangers with either fixed temperature or fixed heat flux) are indistinguishable. The profile obtained from the ideal heat exchanger model is very close to the other two, but a slight difference can be observed in the detail shown in Fig. 6. In any case, these profiles are very different from the linear approximation. The temperature gradient along the stack plates, i.e., ultimately, the gradient available to drive the thermoacoustic instability, is significantly smaller in models that account for a non-zero space between heat-exchangers and stack.

These steady conduction fields mostly depend upon the heat exchanger geometry and the relative thermal conductivities of the solid(s) and the fluid. (That these conductivities depend upon temperature has not been taken into account.)

Amplification

Several simulations of the initial amplification phase have been performed, corresponding to three mean pressure conditions, a given temperature difference imposed between heat exchangers, and in some cases, different values of the impedance (load).

For mean pressure, and temperature difference, the choice was based upon the reference experiment [8]. In some cases, the impedance (f) was chosen so that the amplification was clearly visible. Relating this value of the load impedance to the experiment is complex; this is currently under study.

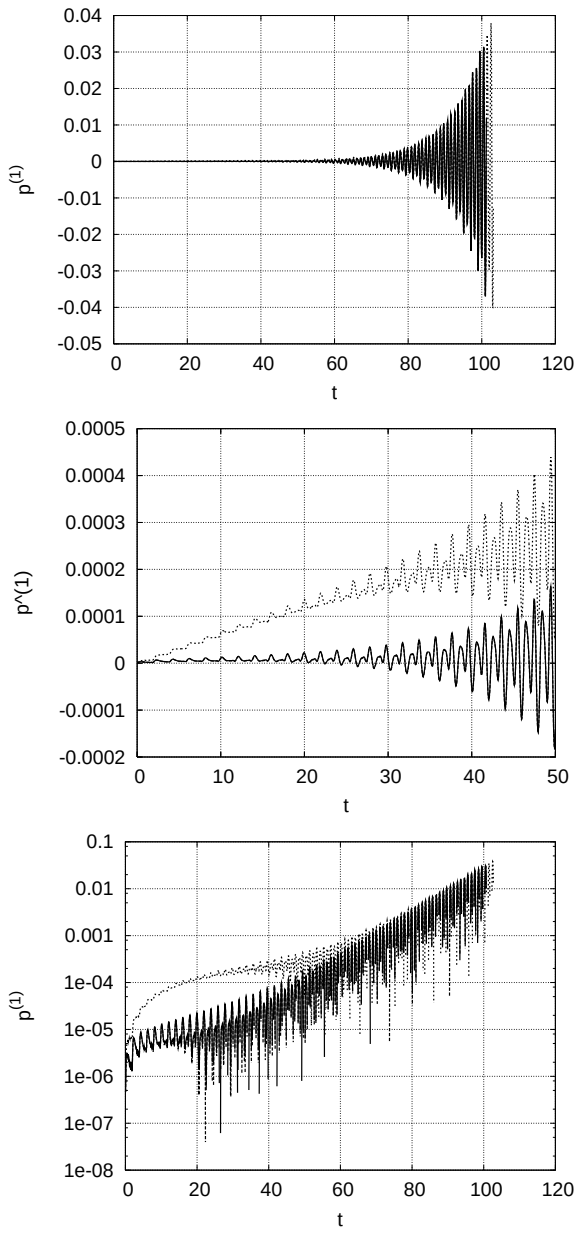

FIGURE 7. $\tilde{p}_{ref} = 150kPa$, time history of acoustic pressure for the three heat-exchanger models. Top: entire run; Middle: detail at beginning of run; Bottom: entire run, log-lin scale

Effect of the heat exchanger model. A comparison of the three exchanger models is shown in Fig. 7 (time history of the acoustic pressure) and Fig. 8 (time history of the axial velocity at the right side of the heat exchanger section). This comparison was performed for the case $\Delta T = 450K$, $\tilde{p}_{ref} = 1.5 \times 10^5 Pa$, with a load kept at a constant value $f = 100$. The results obtained for the two models with solid plates and either temperature or heat flux prescribed, are superimposed on the figures. The results obtained for the "ideal" heat exchanger model are slightly different, especially for pressure and initially, which starts by deviating slightly from zero, Fig. 7 (middle). Later in the amplification process, this deviation disappears, and the acoustic pressure term $p^{(1)}$ returns to an oscillation around 0. If plotted on a log-lin scale, the linear part of the curves are almost parallel, showing that the growth rates are very close.

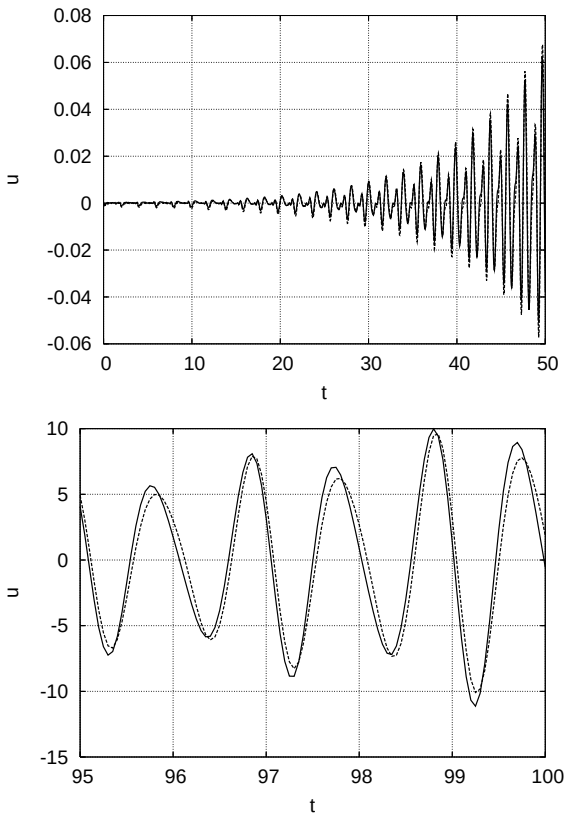

FIGURE 8. $\tilde{p}_{ref} = 150kPa$, time history of axial velocity at right of the heat exchanger section, for three heat-exchanger models

At higher pressure $\tilde{p}_{ref} = 4.4 \times 10^5 Pa$, but otherwise the same values as above, $\Delta T = 450$K and load $f = 100$, a comparison between the three exchanger models is shown in Fig. 9 (time history of acoustic pressure). The reference fluid density is now three times the previous one. In this case, the two models with solid plates and either temperature or heat flux prescribed still give almost identical results, but the ideal heat exchanger model now shows amplification occurring later than the other two models. However, the growth rates, as seen in Fig. 9 (bottom) on the log-lin plot, are very similar.

This is a little surprising since ideal exchangers should intuitively drive larger amplification. However, the driving term at each time step comes from integrating the heat flux over the

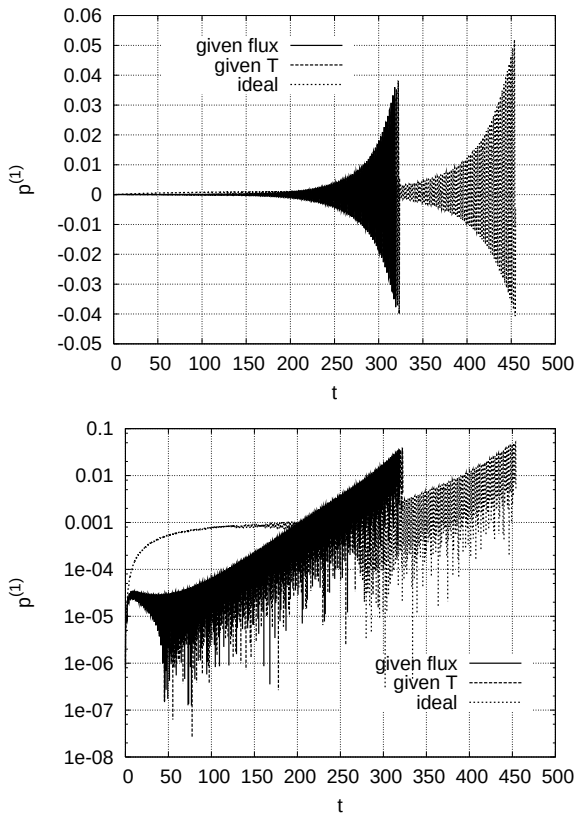

FIGURE 9. $\tilde{p}_{ref} = 440kPa$, time history of acoustic pressure for the three heat-exchanger models, starting from heat conduction temperature field, $f = 100$

entire heat exchanger section, and in the case of the ideal heat exchanger, only the plates contribute to the heat flux. The model used here may not be the adequate model for ideal exchange.

Unstable Mode Selection. Results shown in Fig. 10, 11 and 12 correspond to simulations at three different mean pressures, $\tilde{p}_{ref} = 4.4 \times 10^5 Pa$, $2.4 \times 10^5 Pa$ and $1.5 \times 10^5 Pa$. The heat exchanger conditions were set so that the temperature difference between the hot and the cold heat exchanger was 450K in all cases. Initial temperature fields corresponded to the steady heat conduction temperature distribution described in the previous section. The value of the load f was chosen such that the initial amplification is clearly visible, and thus a different value was chosen in each case. For higher mean pressure, $\tilde{p}_{ref} = 4.4 \times 10^5 Pa$, Fig. 10, the most unstable mode is very close to the fundamental in a tube at ambient (cold) temperature, with period of oscillations close to 2 in the current scaling. For the lower value of the mean pressure, $\tilde{p}_{ref} = 1.5 \times 10^5 Pa$, Fig. 11, the most unstable mode is close to the first harmonic, with period of oscillations close to 1. For the intermediate value

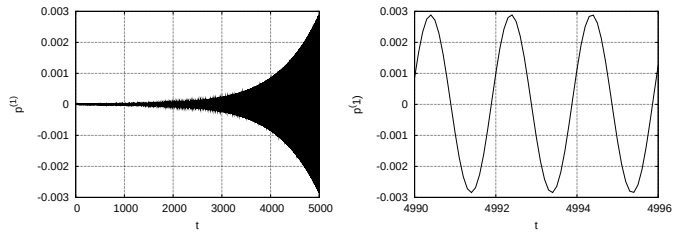

FIGURE 10. $\tilde{p}_{ref} = 440kPa$, time history of acoustic pressure (detail on right figure)

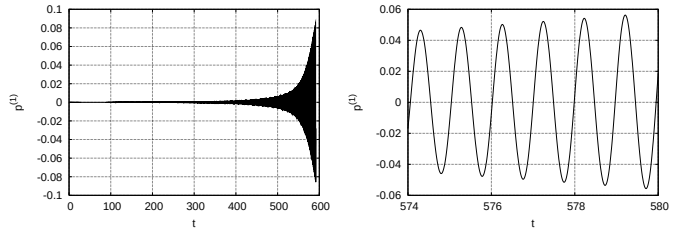

FIGURE 11. $\tilde{p}_{ref} = 150kPa$, time history of acoustic pressure (detail on right figure)

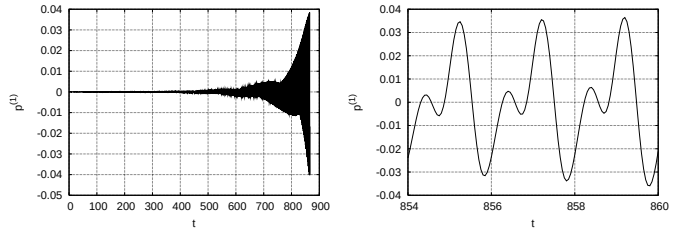

FIGURE 12. $\tilde{p}_{ref} = 240kPa$, time history of acoustic pressure (detail on right figure))

of the mean pressure, $\tilde{p}_{ref} = 2.4 \times 10^5 Pa$, Fig. 11, both the fundamental and the first harmonic are unstable. These results are in agreement with marginal curves obtained by [8]. These curves show the instability of the fundamental and harmonic modes as a function of ΔT and $\tilde{p}_{ref}$, indicating the presence of 3 zones. For high mean pressure, only the fundamental is unstable, for low mean pressure, the first harmonic is the most unstable, and for a narrow range of intermediate mean pressure, both fundamental and harmonic modes are unstable. Current results are consistent.

CONCLUSION

Direct simulation of a complete thermoacoustic engine was performed. Based upon a multiple scale analysis, the global compressible flow problem is reduced to a dynamically incompress-

ible problem in the heat exchangers, with boundary conditions derived from linear acoustics in the resonator.

Three models of heat exchangers were implemented, yielding similar results. The model was used to study several features of the engine, including the influence of the mean pressure. Results show that the approach will yield valuable information on the operation of the engine, which remains otherwise rather opaque. While the current approach still requires relatively large simulations, as the current results show, it is possible to use the model in a parametric study, which will help understanding trade offs.

ACKNOWLEDGMENT

Support of the Natural Sciences and Engineering Research Council of Canada is gratefully acknowledged (LB).

Computations were performed on the NEC-SX8 of the IDRIS-CNRS computing center, under project No. i2009020599.

REFERENCES

[1] N. Rott, "Damped and thermally driven acoustic oscillations in wide and narrow tubes", Z. Angew. Math. Phys., 230-243, (1969).

[2] N. Rott, "Damped and thermally driven acoustic oscillations in wide and narrow tubes. Part II : Stability limits for Helium." Z. Angew. Math. Phys., 54-72, (1972).

[3] G. W. Swift, "Thermoacoustic engines", J. Acoust. Soc. Am. **84**, 1145-1180 (1988).

[4] E. Besnoin and O. Knio, Numerical study of thermoacoustic heat exchangers, Acta. Acust. Acust. **90**, 432444, (2004).

[5] D. Marx and Ph. Blanc-Benon, Numerical simulation of the stack-heat exchangers coupling in a thermoacoustic refrigerator, AIAA J. **42**, 1338-1347, (2004).

[6] A. Berson and Ph. Blanc-Benon, Nonperiodicity of the flow within the gap of a thermoacoustic couple at high amplitudes, J. Acoust. Soc. Am. **122** (4), 3014 (2007).

[7] O. Hireche, C. Weisman, D. Baltean-Carlès, P. Le Quéré and L. Bauwens, "Analysis and Simulation of Thermoacoustic Engine", Comptes Rendus (Mécanique), **338**, 18-23(2010).

[8] A.A Atchley and F. M. Kuo, "Stability curves for a thermoacoustic prime mover", J. Acoust. Soc. Am. **95**, 1401-1404 (1994).

[9] L. Bauwens, "Oscillating flow of a heat-conducting fluid in a narrow tube", J. Fluid Mech. **324**, 135-161 (1996).

[10] S. Paolucci, "On the filtering of sound from the Navier-Stokes equations", Sandia National Laboratories report SAND82-8257 (1982).

[11] A. Majda and J.A. Sethian, "The derivation and numerical solution of the equations for zero Mach number combustion", Combust. Sci. Tech. **42**, 185-205 (1984).

[12] P. Le Quéré, R. Masson, and P. Perrot, "Chebyshev collocation algorithm for 2D non Boussinesq convection", J. Comp. physics, vol. **103**, 320-335 (1992).